

# A Variable-Slope Smooth- $k$ Filter for Modeling Halo Abundances with Damped and Oscillatory Power Spectra

Andreu Rocamora Martorell <sup>\*</sup>

Facultat de Física, Universitat de Barcelona, Martí Franquès 1, E-08028 Barcelona, Spain

**ABSTRACT.** We introduce a variable-slope smooth- $k$  (VSMK) filter within the Press-Schechter formalism to model halo mass functions derived from damped and oscillatory matter power spectra. While the standard smooth- $k$  approach successfully captures small-scale suppression effects, it intrinsically couples these to oscillatory features at intermediate scales. The VSMK filter generalizes this framework by allowing the effective logarithmic slope of the  $k$ -space window function to vary smoothly between two asymptotic regimes, thereby decoupling the small-scale suppression of halo abundances from the intermediate-scale oscillatory features characteristic of dark acoustic oscillations. We compare the analytic predictions obtained with the VSMK filter to  $N$ -body simulations for warm dark matter and ETHOS-based models, showing that a single parameter set reproduces both regimes simultaneously. The VSMK filter thus provides a unified and flexible analytic framework for modeling halo abundances in non-cold dark matter scenarios with damped and oscillatory power spectra.

**Keywords:** cosmology: theory – dark matter – large-scale structure of the Universe

## 1 Introduction

Dark matter constitutes the dominant component of the matter content of the Universe, yet its fundamental nature remains one of the central open problems in modern cosmology. The cold dark matter (CDM) paradigm [1] has been remarkably successful in describing the abundance of massive cosmic structures, as well as a wide range of large-scale observables [2, 3]. However, on galactic and sub-galactic scales, CDM faces a number of well-known challenges, including the missing satellites problem [4, 5], the core–cusp problem [6], and the too-big-to-fail problem [7]. For comprehensive reviews, see [4, 8].

Motivated by these small-scale tensions, a broad class of alternative dark matter models has been proposed over the past decades. Many of these scenarios predict a suppression of structure formation on small scales, typically reflected as a cutoff or damping feature in the halo mass function (HMF). In most cases, this suppression originates from physical processes acting after inflation. Examples include free streaming induced by non-negligible thermal velocities, as in warm dark matter (WDM) models [9, 10, 11, 12]; collisional interactions between dark matter and relativistic species, which can give rise to dark acoustic oscillations (DAO) [13, 14]; and the quantum wave-like nature of dark matter in fuzzy dark matter (FDM) models [15, 16, 17, 18].

Current observational constraints on the HMF increasingly push the characteristic suppression scale toward lower halo masses, thereby placing progressively stronger bounds on the minimum

---

<sup>\*</sup>Email: andreu.rocamora@ceab.csic.es  
Date: February 1, 2026

dark matter particle mass [19, 20, 21]. As a result, potentially observable deviations from the CDM prediction are expected to occur at masses  $\leq 10^7 M_\odot$ . Probing this regime requires increasingly sensitive observational techniques, including strong gravitational lensing [22, 23, 24, 25, 26], perturbations of stellar streams [27, 28, 29], and neutral hydrogen (HI) surveys [30, 31, 32].

In practice, numerical simulations are often employed to study the HMF in this mass range. However, simulations face significant challenges at small scales, as low-mass halos can only be reliably identified once they contain a sufficiently large number of particles, giving rise to the well-known issue of spurious halo formation (e.g. [33, 16, 34]). From an analytical perspective, the extended Press-Schechter (EPS) formalism [35, 36, 37] provides a flexible framework to model the HMF in CDM [38, 39], WDM [40, 33], DAO [13, 14, 41], and FDM scenarios [42, 43].

The role of density-field filtering in shaping the HMF within the EPS formalism has been extensively studied over the past three decades [36]. More recently, it has been shown that, for models with a damped linear matter power spectrum, such as WDM or DAO, the small-scale behavior of the HMF is strongly sensitive to the choice of filter [14, 44]. In this context, Leo et al. introduced the smooth- $k$  space (SMK) filter [34], which provides additional freedom to control the small-mass logarithmic slope, hereafter referred to as *slope*, of the halo mass function. The SMK filter has been shown to successfully reproduce WDM halo abundances across a range of cosmological parameters [45, 14].

However, recent studies employing the effective theory of structure formation (ETHOS) framework [46] have highlighted important limitations of the SMK filter when applied as a universal prescription for both WDM and DAO models [14, 41]. These limitations arise because the slope of the SMK filter is characterized by a single parameter, which simultaneously controls the suppression of the HMF at small masses and the smoothing of oscillatory features at intermediate scales. As a consequence, the damping characteristic of WDM models and the oscillations induced by DAO become intrinsically coupled, preventing an independent adjustment of the small- and intermediate-mass regimes of the HMF. This motivates the question of whether a simple analytic filter can be constructed to treat these regimes separately.

In this work, we address this problem by exploiting a key property of the EPS formalism: in models with truncated or damped power spectra, the HMF at small halo masses is primarily controlled by the filtering of spatial scales larger than the characteristic collapse scale of the halo (i.e. small wavenumbers), whereas the HMF at intermediate masses—where DAO effects are most pronounced—is sensitive to the filter behavior at intermediate and smaller spatial scales. This inversion between the relevant regions of the filter and the corresponding mass scales of the HMF enables the construction of a variable-slope smooth- $k$  (VSMK) filter. By allowing the effective slope of the filter to vary continuously between two asymptotic values, the VSMK filter can independently reproduce both the small-scale suppression of the HMF and the oscillatory features characteristic of DAO.

We therefore propose the VSMK filter as a unified and flexible analytic tool capable of describing halo mass functions in both WDM and ETHOS-based models with DAO using a single set of parameters. Its ability to disentangle the contributions from different physical regimes makes it particularly well suited for future applications, as forthcoming observations [31, 26, 29] and higher-resolution simulations extend reliable HMF measurements to increasingly smaller scales, thereby constraining the small-mass slope of the HMF and enabling a corresponding fit of the filter parameters.

This paper is organized as follows. In Section 2, we summarize the Press-Schechter formalism and the transfer functions used to construct non-CDM power spectra. The variable-slope smooth- $k$  filter is introduced and motivated in Section 3. Our results and comparisons with numerical simulations are presented in Section 4, followed by the conclusions in Section 5.

## 2 The Press-Schechter formalism

The Press-Schechter formalism (PSF) [35, 47], and in particular its extended formulation (EPS) [36, 37, 48, 49, 50], provides an analytic framework to describe several aspects of the non-linear evolution of cosmic structure. The formalism is based on the linear density contrast field  $\delta(\mathbf{x}, t)$  and assumes that density perturbations grow linearly in time according to

$$\delta(\mathbf{x}, t) = \delta_0(\mathbf{x}) D(t), \quad (1)$$

where  $D(t)$  is the linear growth factor, normalized to unity at the present time.

Within this framework, the fraction of mass collapsed into halos of mass  $M$  at redshift  $z$  is identified with the fraction of trajectories of the smoothed density field that exceed a critical threshold for collapse,  $\delta_c(z)$ , when filtered on the mass scale  $M$  [35]. This assumption leads to an expression for the halo mass function (HMF) given by

$$\frac{dn}{d \ln M} = -\frac{1}{2} \frac{\bar{\rho}}{\sigma^2(M)} f(\nu) \frac{d\sigma^2(M)}{dM}, \quad (2)$$

where  $n$  denotes the comoving number density of halos,  $\bar{\rho}$  is the mean matter density of the Universe, and  $f(\nu)$  is the first-crossing distribution.

Assuming ellipsoidal collapse [51], the first-crossing distribution is well described by

$$f(\nu) = A \sqrt{\frac{2q\nu}{\pi}} [1 + (q\nu)^{-p}] \exp\left(-\frac{q\nu}{2}\right), \quad (3)$$

with fiducial parameter values  $A = 0.322$ ,  $q = 0.707$ , and  $p = 0.3$ . When comparing the analytical model with the simulations of [52] (Fig 4), we adopt  $A = 0.3658$ , consistent with the calibration reported in that work.

The dimensionless peak-height parameter  $\nu$  is defined in terms of the critical overdensity for spherical collapse as

$$\nu = \frac{\delta_c^2(0)}{\sigma^2(R) D^2(z)}, \quad (4)$$

where  $\delta_c(0)$  is the present-day linear collapse threshold,  $\sigma^2(R)$  is the variance of the density field on the scale  $R$ , and  $D(z)$  is the linear growth factor evaluated at redshift  $z$ .

The variance of the density perturbations on the scale  $R$  is given by

$$\sigma^2(R) = \frac{1}{2\pi^2} \int_0^\infty k^2 P(k) W^2(k, R) dk, \quad (5)$$

where  $k$  denotes the wavenumber,  $P(k)$  is the linear matter power spectrum of the considered model, and  $W(k, R)$  is a spherically symmetric Fourier-space window function for the scale  $R$ .

### 2.1 Density-field filters

Window functions, also known as filters, define how density perturbations are weighted as a function of distance from a given point in order to determine whether a halo of mass  $M$  collapses. For a halo with a given characteristic scale  $R$  and mass  $M$ , the filtering procedure suppresses the contribution of perturbations on scales smaller than the halo size. In Fourier space, this corresponds to weighting the modes that compose the density contrast field, such that

$$\delta(k, R) = \hat{\delta}(k) W(k, R), \quad (6)$$

where  $\hat{\delta}(k)$  is the Fourier transform of  $\delta(x)$ , and  $W(k, R)$  is a window function associated with the scale  $R$ .

The simplest choice of window function is the real-space top-hat (TH) filter,

$$W_{\text{TH}}(r, R) = \Theta(1 - r/R), \quad (7)$$

whose main advantage lies in its straightforward physical interpretation: it selects all the mass contained within a sphere of radius  $R$ , leading to a direct relation between mass and scale,  $M = (4/3)\pi\bar{\rho}R^3$ . However, the TH filter does not provide an accurate description of the halo mass function in CDM [36], nor in models with a damped linear power spectrum, where it predicts an unphysical upturn of the HMF at low masses that is not observed in numerical simulations [44].

A simple alternative that improves the agreement with simulations is the sharp- $k$  space (SHK) filter introduced in [36],

$$W_{\text{SHK}}(k, R) = \Theta(1 - kR). \quad (8)$$

By imposing a sharp cutoff in Fourier space, this filter successfully reproduces the suppression of the HMF in warm dark matter universes [44, 33]. Nevertheless, while the SHK filter induces a decline of the HMF at small masses, the slope of this decline is fixed and cannot be tuned.

To allow for greater flexibility in the small-scale behavior of the HMF, the smooth- $k$  space (SMK) filter was proposed in [34],

$$W_{\text{SMK}}(k, k_M^{-1}) = \left[ 1 + \left( \frac{k}{k_M} \right)^\beta \right]^{-1}, \quad (9)$$

where  $k_M = 1/R$ . In models with a damped power spectrum, the SMK filter yields a halo mass function that asymptotically follows

$$\frac{dn}{d \ln M} \propto M^{(\beta-3)/3} \quad (10)$$

at small masses (see Section 3).

Motivated by this behavior, and in order to disentangle the contributions of different mass regimes in the HMF, we propose a filter that interpolates between two SMK-like behaviors: an effective slope  $\beta_1$  for  $k/k_M \ll 1$  and a slope  $\beta_2$  for  $k/k_M \gg 1$ . The explicit functional form of this variable-slope smooth- $k$  (VSMK) filter, together with its derivation and properties, is presented in Section 3 (see also Figure 1).

The definition of halo mass is not straightforward for filters such as SHK and SMK, since their real-space counterparts have divergent integrals. To circumvent this issue, it is customary to assume that the mass scale obeys  $M \propto R^3$  owing to the spherical symmetry of the filtering procedure, and to define

$$M = \frac{4\pi}{3} \bar{\rho} (cR)^3, \quad (11)$$

where  $c$  is a free parameter calibrated against numerical simulations. This parameter has been shown to improve the agreement between analytic predictions and simulations for the HMF [34, 13, 14, 41], halo concentrations [53]—using procedures such as those described in [54, 55]—and the slope of the Einasto density profile [53].

Varying  $c$  effectively shifts the halo mass function along the mass axis, without altering its asymptotic slopes or its sensitivity to specific features of the linear power spectrum. In this sense,  $c$  plays the same role in the VSMK filter as in the standard SMK case, and should be regarded as a mass calibration parameter rather than a shape parameter of the filter. Formally, this follows from the fact that the parameter  $c$  does not enter the window function  $W(k, R)$  itself, but only the relation between halo mass and the characteristic wavenumber,  $k_M = R^{-1}$ . As a result, varying  $c$  changes

the value of  $k_M$  at which the variance is evaluated, but does not modify the relative weighting of Fourier modes within the variance integral. This behavior is therefore qualitatively different from that of the slope parameters  $\beta_1$  and  $\beta_2$  (Section 3), which explicitly alter the functional form of the filter and control how oscillatory features of the power spectrum are smoothed.

Originally, a value  $c \simeq 2.42$  was proposed for the SHK filter [56]. Subsequent studies found that values in the range  $c = 2.5\text{--}2.7$  provide a better fit for SHK-based models [33]. More recently, analyses employing the SMK filter have identified a preferred range  $c = 3\text{--}3.7$  [34, 13, 14, 41].

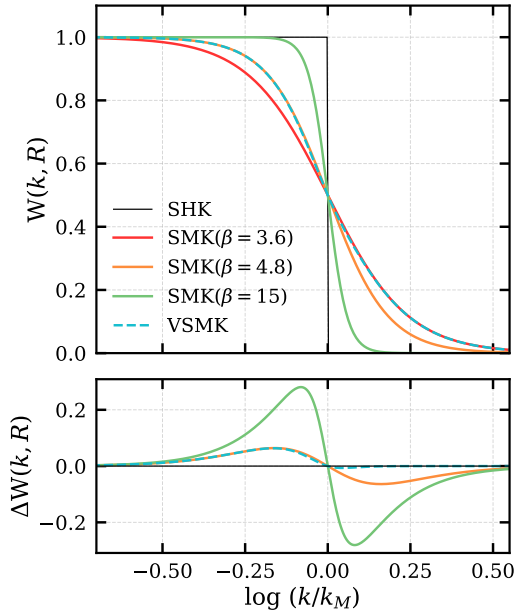


**Figure 1: Comparison between smooth- $k$  (SMK) and variable-slope smooth- $k$  (VSMK) filters.** The SMK filter is shown for different values of the slope parameter  $\beta$  and compared to a VSMK filter with  $\beta_1 = 4.8$ ,  $\beta_2 = 3.6$ ,  $\delta = 12$ , and  $\mu = 1$ , chosen for illustrative purposes. In all cases,  $c = 1$  is also adopted for visualization only. The lower panel shows the difference  $\Delta W(k, R) = W(k, R) - W_{\text{SMK}(\beta=3.6)}(k, R)$  for each filter.

## 2.2 Linear power spectra in non-CDM models

The linear matter power spectrum of a non-cold dark matter model can, in general, be expressed in terms of a transfer function  $T(k)$  as

$$P_i(k) = P_{\text{CDM}}(k) T^2(k), \quad (12)$$

where  $P_{\text{CDM}}(k)$  is the linear CDM power spectrum and  $P_i(k)$  denotes the corresponding non-CDM spectrum. The CDM power spectrum used in this work is computed with the CAMB code [57].

A unified description of a wide class of transfer functions was proposed in [58] and subsequently adopted as the basis for the ETHOS framework [59]. The ETHOS transfer function [46, 60], as derived in [59], allows one to describe warm dark matter-like suppression as well as the presence of dark acoustic oscillations (DAO) in a single parametrized form [59, 52, 41].

In this work, we model the linear power spectrum of WDM using the standard transfer function introduced in [11],

$$T_{\text{WDM}}(k) = [1 + (\alpha k)^{2\nu}]^{-5/\nu}, \quad (13)$$

with  $\nu = 1.12$  [12]. The parameter

$$\alpha = 0.049 \left( \frac{m_{\text{WDM}}}{1 \text{ keV}} \right)^{-1.11} \left( \frac{\Omega_m}{0.25} \right)^{0.11} \left( \frac{h}{0.7} \right)^{1.22} \quad (14)$$

sets the characteristic scale of the suppression, while  $\nu$  controls its shape.

For models featuring dark acoustic oscillations, we adopt the ETHOS transfer function presented in [59],

$$T_{\text{ETHOS}}(k) = [1 + (\alpha k)^\beta]^\gamma - \sqrt{h_{\text{peak}}} \exp \left[ -\frac{1}{2} \left( \frac{x-1}{\Sigma} \right)^2 \right] + \frac{\sqrt{h_2}}{4} \operatorname{erfc} \left( \frac{x-x_0}{\tau} - 2 \right) \operatorname{erfc} \left( -\frac{x-x_0}{\Sigma} - 2 \right) \cos(1.1083\pi x), \quad (15)$$

where  $x \equiv k/k_{\text{peak}}$ ,  $x_0 = 1.805$ , and  $\Sigma = 0.2$ . The parameter  $\alpha$  plays a role analogous to the suppression scale in Eq. (13), while  $\beta$  and  $\gamma$  determine the shape of the suppression. The parameters  $h_{\text{peak}}$  and  $k_{\text{peak}}$  control the amplitude and characteristic scale of the first DAO peak, respectively, and  $h_2$  sets the amplitude of the second oscillation.

Within this generalized formalism, all parameters are uniquely determined by the pair  $(h_{\text{peak}}, k_{\text{peak}})$ . In particular, the limit  $h_{\text{peak}} = 0$  recovers the WDM-like transfer function in Eq. (13), while the limit  $k_{\text{peak}} \rightarrow \infty$  yields  $T(k) \rightarrow 1$ , corresponding to the CDM power spectrum.

Following [59], the parameter  $\alpha$  can be expressed as

$$\alpha = \frac{d}{k_{\text{peak}}} \left[ \left( \frac{1}{\sqrt{2}} \right)^{1/\gamma} - 1 \right]^{1/\beta}, \quad (16)$$

where the parameters  $d$  and  $\beta$  depend on  $h_{\text{peak}}$ , and  $\gamma = -20$ . Explicit values for representative cases are provided in Table 1, following [59] and the interpolation scheme of [41].

Finally, within the ETHOS framework, the WDM particle mass can be related to the ETHOS peak scale through [12, 59]

$$\frac{m_{\text{WDM}}}{1 \text{ keV}} = \left[ 0.050 \left( \frac{k_{\text{peak}}}{h \text{ Mpc}^{-1}} \right) \left( \frac{\Omega_\chi}{0.25} \right)^{0.11} \left( \frac{h}{0.7} \right)^{1.22} \right]^{1/1.11}. \quad (17)$$

**Table 1:** Parameters used to construct the linear matter power spectra within the ETHOS framework, as a function of the amplitude  $h_{\text{peak}}$  of the first dark acoustic oscillation. Only the representative cases  $h_{\text{peak}} = 0.0$ , 0.4, and 1.0 from [59] are shown.

$h_{\text{peak}}$	$h_2$	$\tau$	$\Sigma$	$\beta$	$d$
0.0	0.0	0.0	0.0	2.24	3.0
0.4	$0.221 \exp(-0.025k_{\text{peak}}) + 0.0129$	0.34	0.22	3.61	2.61
1.0	1.08	0.67	0.2	4.05	2.5

### 3 The variable slope smooth- $k$ filter

The standard SMK filter does not allow for an independent control of the low-mass and high-mass regimes of the HMF. As a consequence, it cannot simultaneously reproduce both the small-scale suppression characteristic of models with a damped matter power spectrum and the oscillatory features induced by dark acoustic oscillations (see Fig. 2).

To construct a more general filter capable of capturing both effects, we exploit a fundamental property of the Press-Schechter formalism. For models with a damped linear power spectrum, the asymptotic slope of the HMF at small masses is determined by the behavior of the filter in the regime  $k/k_M \ll 1$ . At large masses, the HMF is largely insensitive to the filter and mainly set by the shape of the power spectrum. However, in models exhibiting oscillatory features, such as DAO scenarios, the HMF can retain a residual dependence on the filter around intermediate wavenumbers, typically  $k/k_M \gtrsim 1$ . These observations, discussed in detail in Appendix A, motivate the introduction of a filter with independently tunable slopes in these two regimes.

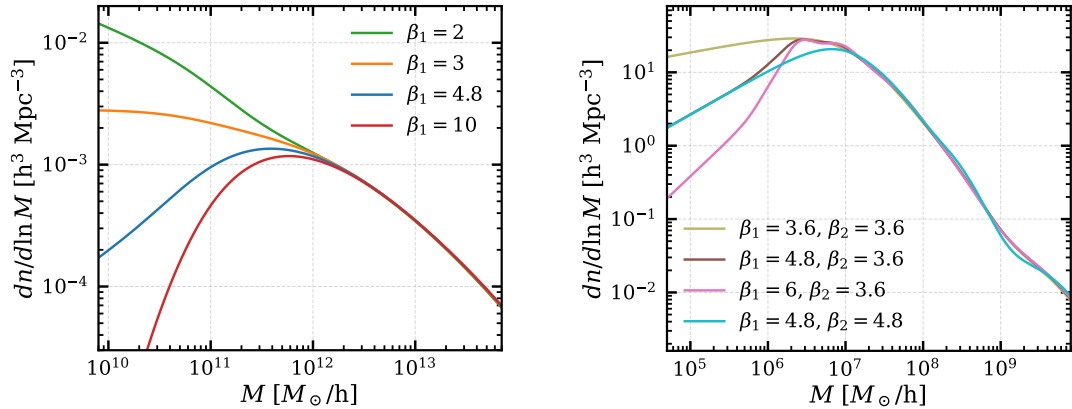


**Figure 2: Impact of the VSMK filter parameters on the halo mass function.** Both panels show halo mass functions computed using the variable-slope smooth- $k$  (VSMK) filter with fixed  $\mu = 2.1$ ,  $\delta = 12$ , and  $c = 3.6$ . *Left:* WDM-like power spectrum with fixed  $\beta_2 = 3.6$  and varying  $\beta_1$ , illustrating that  $\beta_1$  exclusively controls the small-mass slope of the HMF. *Right:* DAO power spectrum with simultaneous variations of  $\beta_1$  and  $\beta_2$ , demonstrating that  $\beta_1$  regulates the small-mass behavior, while  $\beta_2$  controls the intermediate-mass regime where DAO-induced oscillations are present.

For sufficiently small masses in models with a damped power spectrum (i.e. WDM or DAO), the variance of the density field asymptotically approaches a constant value [44, 33]. In this regime, one finds  $dn/d \ln M \propto d\sigma^2/dk_M$  [44, 34]. The derivative of the variance with respect to  $k_M$  is given by

$$\frac{d\sigma^2(R)}{dk_M} = \frac{1}{2\pi^2} \int_0^\infty \xi(k, k_M) dk, \quad (18)$$

where the integrand is

$$\xi(k, k_M) \equiv k^2 P(k) \frac{\partial W^2(k, R)}{\partial k_M} = 2k^2 P(k) W(k, R) \frac{\partial W(k, R)}{\partial k_M}. \quad (19)$$

For the SMK filter, the integrand  $\xi(k, k_M)$  exhibits a pronounced maximum in the regime  $k/k_M \ll 1$  when  $k_M \gg k_{\text{hm}}$ , where  $k_{\text{hm}}$  denotes the half-mode scale at which the HMF is suppressed by a factor of two relative to CDM. As the mass decreases, this maximum becomes increasingly localized, allowing the integral in Eq. (18) to be approximated around its peak (Appendix A.1).

Since the VSMK filter asymptotically reduces to the SMK form in this regime (see Fig. 1), the same argument applies to both filters.

Expanding the SMK filter,  $W_{SMK} \equiv W_{SMK}(k, R)$ , at leading non-vanishing order for  $k/k_M \ll 1$ , one obtains

$$W_{SMK} = 1 - \left( \frac{k}{k_M} \right)^\beta + \mathcal{O}[(k/k_M)^{2\beta}], \quad (20)$$

with the analogous expansion for the VSMK filter (Eqs. (23) and (24)),

$$W_{VSMK} = 1 - \left( \frac{k}{k_M} \right)^{\beta_1} + \mathcal{O}[(k/k_M)^{2\beta_1}]. \quad (21)$$

Substituting these expressions into Eqs. (18) and (19) yields  $d\sigma^2/dk_M \propto k_M^{-(\beta_1+1)}$ , where  $\beta_1$  is replaced by  $\beta$  for the SMK filter. Therefore,  $\sigma^2(R) = \sigma_0^2 + Ck_M^{-\beta_1}$ , consistently recovering the constant-variance limit at small scales. Using the scaling  $M \propto k_M^{-3}$ , the asymptotic behavior of the HMF becomes

$$\frac{dn}{d \ln M} \propto k_M^{3-\beta_1} \propto M^{(\beta_1-3)/3}, \quad (22)$$

in agreement with previous results for the SMK filter [14]. This expression is valid up to  $\beta_1 \lesssim 22 - n_s$  for the power spectrum obtained using Viel's transfer function (13); for larger values, the asymptotic behavior converges to that of the sharp- $k$  filter,  $dn/d \ln M \propto k_M^6 P_{WDM}(k_M \rightarrow \infty)$  [44].

At larger masses ( $k_M < k_{hm}$ ), the maximum of  $\xi(k, k_M)$  shifts toward  $k/k_M \sim 1$ , and the previous approximation no longer applies. In this regime, the HMF is largely insensitive to the filter and primarily determined by the shape of the linear power spectrum (Appendix A.2). However, when the power spectrum exhibits oscillatory features, the filter plays a crucial role in smoothing these oscillations, thereby regulating their imprint on the HMF [14]. Consequently, the HMF acquires a dependence on the filter around intermediate wavenumbers,  $k/k_M \gtrsim 1$  (Appendix A.3).

These considerations motivate the definition of the variable-slope smooth- $k$  (VSMK) filter,

$$W_{VSMK} = \left[ 1 + \left( \frac{k}{k_M} \right)^{f(k)} \right]^{-1}, \quad (23)$$

where the effective slope  $f(k)$  interpolates between two asymptotic values,

$$f(k) = \beta_2 - (\beta_2 - \beta_1) \left[ 1 + \left( \mu \frac{k}{k_M} \right)^\delta \right]^{-1}. \quad (24)$$

In this parametrization,  $\beta_1$  governs the small-scale suppression of the HMF, while  $\beta_2$  controls the intermediate-mass regime where DAO-induced oscillations are relevant. The parameter  $\mu$  sets the characteristic transition scale in units of  $k_M$ , and  $\delta$  determines the sharpness of the transition. Larger values of  $\delta$  correspond to a more abrupt change of slope, whereas smaller values produce a smoother interpolation. Accordingly,  $\mu$  and  $\delta$  do not affect the asymptotic behavior of either regime and are therefore treated as fitting parameters controlling the transition only. In this way, this construction introduces the minimal number of additional parameters required to independently control both regimes. As illustrated in Figs. 1 and 2, it allows the two asymptotic regimes of the filter to map directly onto two distinct regimes of the HMF.

## 4 Comparison with $N$ -body simulations

To assess the performance of the variable-slope smooth- $k$  (VSMK) filter, we compare halo mass functions computed within the Press-Schechter formalism with  $N$ -body simulations from Refs. [14],

[52, 41]. These simulations adopt cosmological parameters consistent with *Planck* 2018 results [61]. In particular, the parameter values  $\Omega_m = 0.321$ ,  $\Omega_\Lambda = 0.679$ ,  $h = 0.6688$ ,  $n_s = 0.96$ , and  $\sigma_8 = 0.811$  are used when comparing analytic predictions with the simulations of [14, 41], while for the simulations presented in [52], we adopt  $\Omega_m = 0.311$ ,  $\Omega_\Lambda = 0.689$ ,  $h = 0.675$ ,  $n_s = 0.965$ , and  $\sigma_8 = 0.815$ . These works also provide, for each simulated model, the best-fitting parameters of the SMK filter. In particular, for the WDM simulation of [14] the optimal parameters are  $\beta = 4.8$  and  $c = 3.3$ ; for the DAO model of [52],  $\beta = 3.46$  and  $c = 3.79$ ; and for the DAO model of [41],  $\beta = 3.6$  and  $c = 3.6$ .

In both [14] and [41] it has been shown that a single SMK filter cannot simultaneously reproduce both the small-scale suppression characteristic of WDM models and the oscillatory features induced by dark acoustic oscillations. Figure 3 illustrates this limitation and demonstrates that the VSMK filter is able to describe both scenarios using a single set of parameters, namely  $\beta_1 = 4.8$ ,  $\beta_2 = 3.6$ ,  $\mu = 2.1$ ,  $\delta = 12$ , and  $c = 3.6$ . The values of  $\beta_1$  and  $\beta_2$  are motivated by the optimal SMK slopes reported in [34, 14] and [41], respectively. The parameters  $\mu$  and  $\delta$  are kept fixed across all models and redshifts considered in this work, and are not re-optimized for individual simulations. This choice is motivated by the fact that variations in  $\beta_1$  and  $\beta_2$  account for the dominant changes in the halo mass function over the range of models considered here.

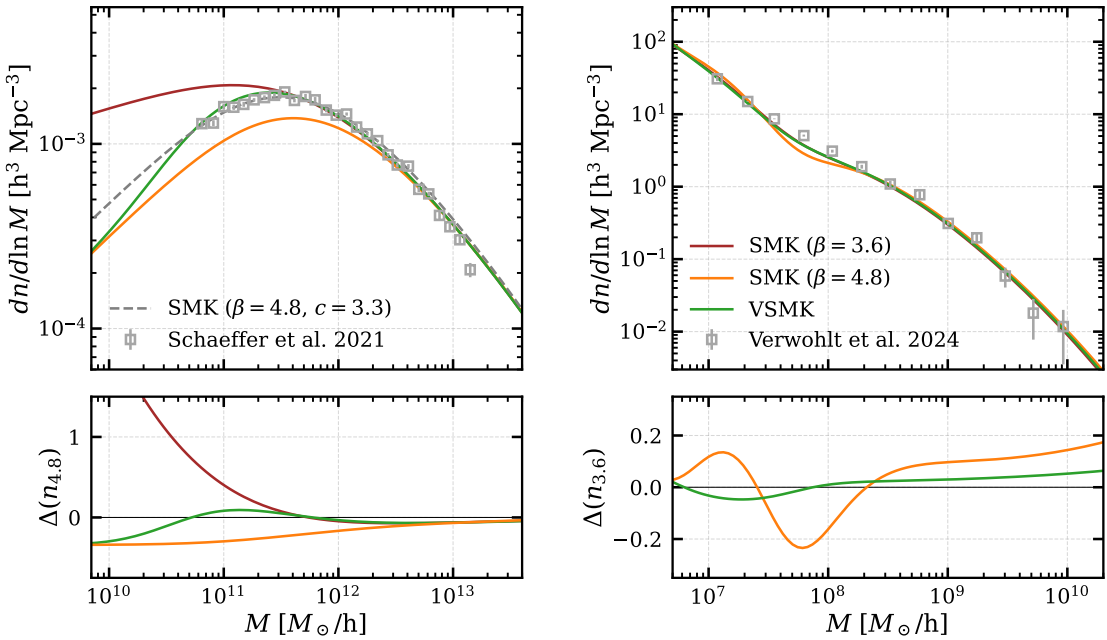


**Figure 3: Comparison between analytical halo mass functions and  $N$ -body simulations for different dark matter models.** The HMFs computed using the optimal SMK filter for each model are compared to those obtained with the SMK filter optimized for the alternative model, as well as with the VSMK filter. Unless stated otherwise,  $c = 3.6$ . *Left:* WDM model with  $m_{\text{WDM}} = 0.25$  keV from [14], where the optimal SMK filter has  $\beta = 4.8$  and  $c = 3.3$  (grey dashed line). *Right:* DAO model with  $h_{\text{peak}} = 1$ ,  $k_{\text{peak}} = 100 h \text{ Mpc}^{-1}$  at  $z = 10$  from [41], where the optimal SMK filter has  $\beta = 3.6$  and  $c = 3.6$ . Simulation data (empty squares) are extracted from published figures in [14] and [41]. The lower panels show the relative deviations  $\Delta$  with respect to the optimal SMK prediction.

The deviation between two halo mass functions is defined as

$$\Delta_i(n_j) \equiv \Delta_i(M, n_j(M)) = \frac{n_i(M) - n_j(M)}{n_j(M)}, \quad (25)$$

where  $n_i(M)$  denotes the HMF computed with the filter under consideration, and  $n_j(M)$  is the reference HMF. When the subscript is a numerical value, it corresponds to the slope  $\beta$  of an SMK filter; when the subscript is VSMK, the VSMK filter with the parameters defined above is used. Here,  $\Delta$  quantifies the relative difference between two analytical halo mass functions, typically comparing the VSMK prediction or a non-optimal SMK filter to the optimal SMK fit for the same model. It is therefore a model-to-model comparison, independent of the simulation data.

For the WDM model shown in Fig. 3, the deviation  $\Delta_{3.6}(n_{4.8}) \rightarrow M^{-0.4} - 1$  as  $M \rightarrow 0$ , in agreement with Eq. (22). In contrast,  $\Delta_{\text{VSMK}}(n_{4.8})$  remains below 0.25 over the full mass range considered, reflecting the fact that the VSMK filter reproduces the correct small-scale asymptotic behavior. For the DAO model, the parameters  $\mu = 2.1$  and  $\delta = 12$  ensure that  $\Delta_{\text{VSMK}}(n_{3.6}) \leq 0.05$  within the resolved mass range,  $10^7 M_\odot \lesssim M \lesssim 10^{10} M_\odot$ , whereas  $\Delta_{4.8}(n_{3.6}) \lesssim 0.25$ .

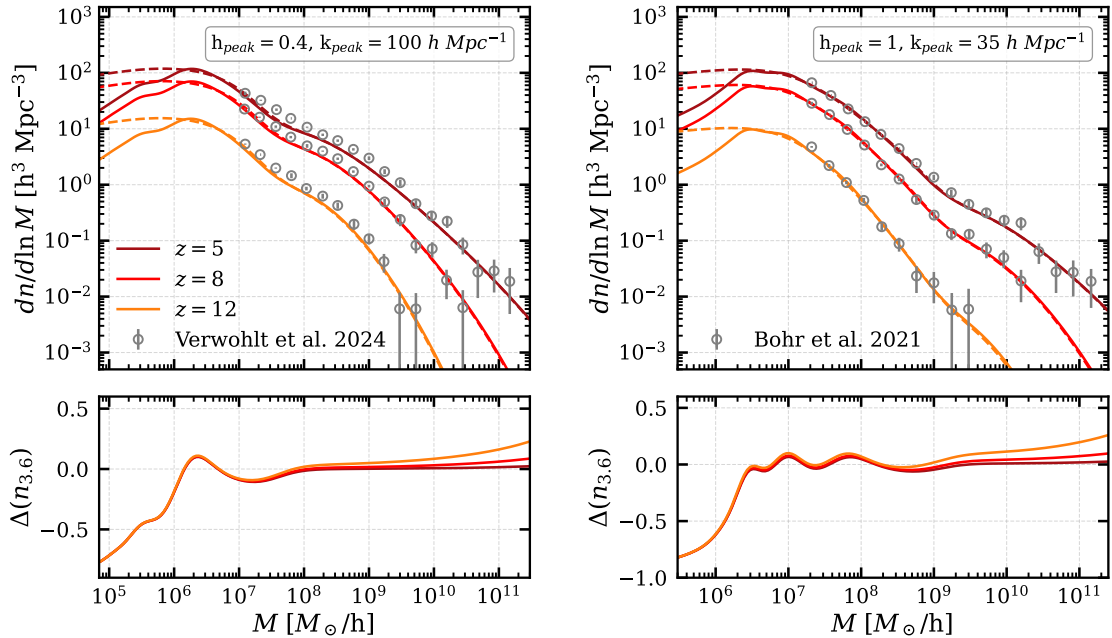


**Figure 4: Comparison between analytical halo mass functions and  $N$ -body simulations at different redshifts for DAO models.** Analytical HMFs (solid lines) computed using the general VSMK filter and the optimal SMK filter are compared to  $N$ -body simulations with similar cosmological parameters from [41, 52] (open circles). *Left:* DAO model from [41], where the optimal SMK filter has  $\beta = 3.6$  and  $c = 3.6$ . *Right:* DAO model from [52], where the optimal SMK filter has  $\beta = 3.46$  and  $c = 3.79$ . Simulation data (empty circles) are extracted from published figures in [41] and [52]. The lower panels show the relative deviations  $\Delta$  with respect to the optimal SMK prediction. Transfer-function parameters are indicated within each panel.

A direct comparison between analytical halo mass functions and the simulation data points (Table 2) further quantifies this improvement. For the WDM model, the mean relative deviations associated with the SMK filter with  $\beta = 3.6$  are approximately a factor of two larger than those obtained with the VSMK filter. For the DAO model, the corresponding deviations for the SMK filter with  $\beta = 4.8$  are approximately 20% larger. In contrast to the relative deviation  $\Delta$ , the errors

reported in Table 2 quantify the agreement between analytical halo mass functions and the  $N$ -body simulation data. These errors are defined as the average relative difference between the analytical predictions and the individual simulation data points.

**Table 2:** Mean relative errors with respect to the  $N$ -body simulation data for the two cases shown in Fig. 3. Deviations for the SMK filter with  $\beta = 4.8$  are computed using the value of  $c$  that provides the best fit for each dark matter model.

	SMK ( $\beta = 4.8, c = 3.3$ )	SMK ( $\beta = 4.8, c = 3.6$ )	SMK ( $\beta = 3.6, c = 3.6$ )	VSMK ( $\beta_1 = 4.8, \beta_2 = 3.6, c = 3.6$ )
WDM	$0.07 \pm 0.09$	-	$0.14 \pm 0.16$	$0.06 \pm 0.07$
DAO	-	$0.22 \pm 0.19$	$0.18 \pm 0.13$	$0.18 \pm 0.16$

Figure 4 shows that the VSMK filter, using the same parameters or only minor adjustments in  $c$  and  $\beta_2$  to match the simulations of [52], provides an accurate description of halo mass functions across different ETHOS models. This result establishes the VSMK filter as a general prescription capable of achieving performance comparable to that of the model-specific optimal SMK filter, while remaining applicable to a broad class of ETHOS scenarios [52, 41]. Within the resolved mass range, we find quantitative agreement at the level of  $\Delta_{\text{VSMK}}(n_i) \leq 0.11$  at  $z = 5$ ,  $\leq 0.1$  at  $z = 8$ , and  $\leq 0.1$  at  $z = 12$ . The figure also highlights the functional separation introduced by the VSMK filter between the large- and small-mass regimes.

## 5 Conclusions

Within the extended Press-Schechter framework, the smooth- $k$  filter has been shown to accurately describe the halo mass function for dark matter models featuring a small-scale suppression in the matter power spectrum. Its single free parameter is sufficient to reproduce the steep decline of the HMF at low halo masses, which is primarily controlled by the behavior of the filter at large spatial scales. This approach, however, becomes insufficient when the power spectrum exhibits multiple physically distinct regimes, such as a sharp suppression at very small scales combined with a damped oscillatory behavior at intermediate scales, as encountered in models with dark acoustic oscillations. In these cases, adjusting the small-mass slope of the HMF through a single SMK parameter inevitably induces an unwanted modification of the intermediate-mass regime, precisely where acoustic oscillations leave their imprint.

To address this limitation, we have introduced the variable-slope smooth- $k$  (VSMK) filter, which makes this scale dependence explicit by allowing for two distinct functional regimes characterized by independent values of the slope parameter. This construction enables a controlled association between the behavior of the filter at large spatial scales and the slope of the HMF at small masses, while the small and intermediate scales of the filter independently regulate the intermediate-mass regime affected by DAO-induced oscillations. In this sense, the VSMK filter makes explicit a scale-inversion mechanism that, in the WDM case, remains hidden due to the simplicity of the underlying power spectrum. From a physical perspective, the variation of the effective slope parameter across mass regimes can be interpreted within the Press-Schechter framework as reflecting the different weights with which density perturbations at distinct scales contribute to the formation of low- and high-mass halos.

The VSMK filter thus constitutes a minimal functional extension of the SMK filter, introducing only the additional degrees of freedom required to interpolate between the relevant regimes. This minimality allows for a consistent treatment of damped and oscillatory power spectra, such as those associated with DAO models, without resorting to model-specific re-calibrations. Although

the current lack of observational constraints and numerical simulations at very low halo masses still limits a full empirical calibration of the filter parameters, the proposed formalism provides a transparent and flexible framework for connecting non-cold dark matter power spectra to predictions for the HMF. This is particularly timely in view of ongoing and forthcoming observational efforts that are beginning to probe increasingly smaller halo mass scales.

## Acknowledgments

The author is especially grateful to Claudi Vall for sustained and in-depth discussions throughout the various stages of this project, which were instrumental in shaping the ideas presented here. The author also acknowledges valuable discussions with Alberto Manrique and Chervin Laporte.

## A Impact of the filter asymptotic behavior on different HMF mass regimes

In Section 3, we showed that the position of the maximum of the integrand  $\xi(k, k_M)$  provides direct insight into the asymptotic behavior of the halo mass function (HMF). This approach can be applied in a particularly transparent way to the small-mass regime of the HMF, as discussed below, while also shedding light on the behavior at intermediate scales for damped and oscillatory power spectra.

### A.1 Filter behavior at $k/k_M \ll 1$ controls the small-mass limit of the HMF

Since the suppression of the HMF at low masses is driven by the small-scale damping of the matter power spectrum—described either by the transfer function in Eq. (13) or by the leading term of Eq. (15)—we consider here a generic power spectrum featuring such a suppression. As a concrete example, the linear power spectrum of a WDM model with  $m_{\text{WDM}} = 0.25 \text{ keV}$ , obtained by applying the transfer function in Eq. (13) to the CDM power spectrum, exhibits the three characteristic asymptotic regimes of damped power spectra [47, 34]:

$$P_{\text{WDM}}(k) \propto \begin{cases} k^{n_s}, & k \lesssim 10^{-2}, \\ k^{-3}, & 10^{-1} \lesssim k \lesssim 1, \\ k^{-24+n_s}, & k \gtrsim 10^1, \end{cases} \quad (26)$$

where the small spatial scale behavior is obtained explicitly in [34].

Although the precise slopes and transition scales differ for ETHOS models, the qualitative behavior of the power spectrum at large wavenumbers is similar. In both WDM and ETHOS scenarios, the small-scale suppression is governed by a term with the same functional form as the leading contribution in Eq. (15). Consequently, the arguments developed below apply generally to ETHOS models and to WDM models with different particle masses, up to numerical differences.

The VSMK filter approaches a SMK filter with  $\beta = \beta_1$  for  $k/k_M < 1/\mu \sim O(1)$ , and a SMK filter with  $\beta = \beta_2$  for  $k/k_M > 1/\mu$  as directly follows from Eqs. (23) and (24). Therefore, to analyze the position and shape of the maximum of  $\xi(k, k_M)$  (19), it is useful to consider the partial derivative of the SMK filter with respect to the inverse of the scale  $k_M = R^{-1}$ , which enters explicitly in the integrand:

$$\frac{\partial W_{\text{SMK}}(k, R)}{\partial k_M} = \frac{\beta (k/k_M)^\beta}{k_M [1 + (k/k_M)^\beta]^2}. \quad (27)$$

This derivative attains its maximum at  $k = k_M$ . Since the filter itself is normalized and bounded between 0 and 1, increasing  $k_M$  shifts this maximum toward progressively smaller physical scales in the power spectrum. When  $k_M$  becomes sufficiently large, i.e.  $k_M \gg k_{\text{hm}}$ , the maximum of the filter derivative lies within the small-scale regime of the power spectrum (e.g.,  $k \gtrsim 10$  in the WDM example above). As a result, the maximum of the integrand  $\xi(k, k_M)$  no longer occurs near  $k/k_M \simeq 1$ , but instead moves to the regime  $k/k_M \ll 1$ , closer to the maximum of the power spectrum itself (see Fig. 5).

For sufficiently steep filter slopes, specifically for  $\beta > 22 - n_s$ , i.e. if the slope of the filter exceeds the absolute value of the slope of  $k^2 P(k)$  obtained from Eq. (13), the decay of the power spectrum is not strong enough to overcome the peak of the filter derivative. In this case, the maximum of  $\xi(k, k_M)$  remains located near  $k \simeq k_M$ , as discussed in the following subsection, and the resulting small-mass behavior of the HMF closely approaches that obtained with a sharp- $k$  filter [44].

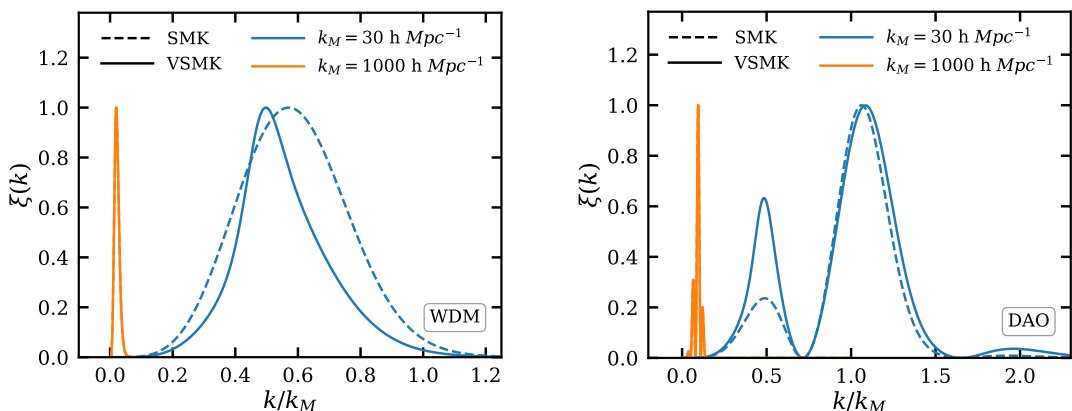


**Figure 5: Normalized integrand of the variance derivative for WDM and DAO models.** The normalized integrands of the variance derivative corresponding to large and intermediate mass scales are presented for the two dark matter models considered in this work. Both the SMK filter (dashed lines), with  $\beta = 4.8$  and  $c = 3.6$  and the VSMK filter (solid lines), with  $\beta_1 = 4.8$ ,  $\beta_2 = 3.6$ ,  $\mu = 2.1$ ,  $\delta = 12$  and  $c = 3.6$  (Section 4) are shown for each model. *Left:* WDM model with  $m_{\text{WDM}} = 1.61 \text{ keV}$ . *Right:* DAO model with  $k_{\text{peak}} = 35 \text{ h Mpc}^{-1}$  and  $h_{\text{peak}} = 1$ . Each integrand is normalized to its own maximum.

## A.2 Independence of the large- and intermediate-mass HMF from the filter in WDM models

At large and intermediate mass scales, the variance  $\sigma^2(R)$  defined in Eq. (5) decreases monotonically as the scale  $R = k_M^{-1}$  increases [33]. In this regime, the first-crossing distribution given by Eq. (3) cannot be treated as constant. Nevertheless, the arguments presented in the previous subsection allow one to identify the dominant contribution to the derivative of the variance.

Specifically, provided that the filter slope satisfies  $\beta > 1$ , the maximum of the integrand  $\xi(k, k_M)$  defined in Eq. (19) lies outside the steeply suppressed small-scale regime and instead coincides with the second asymptotic regime of the linear matter power spectrum. For very small values of  $\beta$ , the absolute value of the slope of  $k^2 P(k)$  overcomes  $\beta$  and the maximum of  $\xi(k, k_M)$  is dominated by the maximum of the power spectrum itself.

In the large- and intermediate-mass regimes, varying the halo mass  $M$  primarily shifts the peak of  $W \partial W / \partial k_M$  along a portion of the power spectrum characterized by a smooth power-law behavior with an approximately constant slope, corresponding to the second regime of the example power spectrum in Eq. (26). As a result, the integral determining  $d\sigma^2/dk_M$  consistently probes the same

region of the filter,  $k/k_M \lesssim 1$ , largely independent of the precise value of  $\beta$  and  $M$ . Combined with the smooth dependence of the first-crossing distribution on  $\sigma^2$  for large and intermediate masses ( $10^8 - 10^{14} M_\odot$ ) [62], this implies that the halo mass function in this regime is weakly sensitive to the choice of filter, as shown in Fig. 2.

In the limiting case  $\beta \rightarrow \infty$ , the smooth- $k$  filter reduces to the sharp- $k$  filter. In this limit, the derivative of the filter becomes a Dirac delta function centered at  $k = k_M$ , so that the derivative of the variance can be evaluated analytically and depends solely on the value of the power spectrum at  $k_M$ . This further illustrates that, for WDM models, the large- and intermediate-mass behavior of the HMF is controlled primarily by the power spectrum rather than by the detailed shape of the filter.

### A.3 Filter dependence of the intermediate-mass HMF in models with oscillatory power spectra

The situation changes qualitatively in models featuring dark acoustic oscillations, where the linear matter power spectrum exhibits damped oscillatory features at intermediate scales. In this case, the dependence of the halo mass function on the filter can be qualitatively understood by extending the arguments presented above.

For a WDM model with  $\beta > 1$ , the integrand  $\xi(k, k_M)$  displays a single dominant peak located near  $k \simeq k_M$  at sufficiently large halo masses. However, in models with oscillatory power spectra, as  $k_M$  increases and intermediate masses are probed, this peak may no longer lie in a region where the power spectrum is smooth. Instead, it coincides with the DAO-induced oscillations, as shown in Fig. 5. Depending on the relative phase, the peak of  $\xi(k, k_M)$  may be enhanced or suppressed, in close analogy with the small-mass regime of WDM models, where the peak is diminished once it enters the steeply damped region of the power spectrum.

As a consequence, oscillatory power spectra can give rise to multiple local maxima in  $\xi(k, k_M)$ . This occurs because the maximum of the filter derivative can remain significant even beyond the first oscillation, since the power spectrum does not decay monotonically but instead partially recovers its amplitude after each oscillation [14, 41]. In this regime, the power spectrum alone no longer uniquely determines the dominant contribution to  $d\sigma^2/dk_M$ ; the detailed shape of the filter becomes equally important.

The role of the filter is to regulate the relative weight of contributions away from the primary peak that would arise in a WDM-like scenario. In particular, the filter smooths the oscillatory features of the power spectrum, thereby controlling the amplitude and persistence of the corresponding oscillations in the halo mass function. In the limiting case  $\beta \rightarrow \infty$ , corresponding again to the SHK filter, the derivative of the filter reduces to a Dirac delta function. As in the WDM case, the derivative of the variance becomes directly proportional to the power spectrum, leading to a highly nonphysical halo mass function that vanishes at masses corresponding to minima of the oscillatory power spectrum [14].

## References

- [1] Peebles, P. J. E. Large-scale background temperature and mass fluctuations due to scale-invariant primeval perturbations. *Astrophysical journal* 263L1-L5, 1982.
- [2] Springel, V., White, S. D., Jenkins, A., Frenk, C. S., Yoshida, N., Gao, L., Navarro, J., Thacker, R., Croton, D., Helly, J., Peacock, J. A., Cole, S., Thomas, P., Couchman, H., Evrard, A., Colberg, J., and Pearce, F. Simulations of the formation, evolution and clustering of galaxies and quasars. *Nature* 435, 2005, 629–636.

- [3] Driver, S. P., Robotham, A. S. G., D., O., Peacock, J. A., Baldry, I. K., Bellstedt, S., Bland-Hawthorn, J., Brough, S., Cluver, M., Holwerda, B. W., Hopkins, A., Lagos, C., Liske, J., Loveday, J., Phillipps, S., and Taylor, E. N. An empirical measurement of the halo mass function from the combination of GAMA DR4, SDSS DR12, and REFLEX II data. *Monthly Notices of the Royal Astronomical Society* 5152, 2022, 2138–2163.
- [4] Weinberg, D. H., Bullock, J. S., Governato, F., Naray, R. K. D., and Peter, A. H. Cold dark matter: Controversies on small scales. *Proceedings of the National Academy of Sciences* 112, 2015, 12249–12255.
- [5] Newton, O., Cautun, M., Jenkins, A., Frenk, C. S., and Helly, J. C. The total satellite population of the Milky Way. *Monthly Notices of the Royal Astronomical Society* 4793, 2018, 2853–2870.
- [6] Walker, M. G. and Peñarrubia, J. A method for measuring (slopes of) the mass profiles of dwarf spheroidal galaxies. *The Astrophysical Journal* 742, 2011, 20.
- [7] Papastergis, E., Giovanelli, R., Haynes, M. P., and Shankar, F. Is there a “too big to fail” problem in the field? *Astronomy & Astrophysics* 574, 2015, A113.
- [8] Bullock, J. S. and Boylan-Kolchin, M. Small-Scale Challenges to the  $\Lambda$ CDM Paradigm. *Annu. Rev. Astron. Astrophys.* 551, 2017, 343–387.
- [9] Shi, X. and Fuller, G. M. New Dark Matter Candidate: Nonthermal Sterile Neutrinos. *Physical Review Letters* 82, 1999, 2832.
- [10] Dodelson, S. and Widrow, L. M. Sterile neutrinos as dark matter. *Physical Review Letters* 721, 1994, 17–20.
- [11] Bode, P., Ostriker, J. P., and Turok, N. Halo Formation in Warm Dark Matter Models. *The Astrophysical Journal* 556, 2001, 93.
- [12] Viel, M., Lesgourgues, J., Haehnelt, M. G., Matarrese, S., and Riotto, A. Constraining warm dark matter candidates including sterile neutrinos and light gravitinos with WMAP and the Lyman- $\alpha$  forest. *Physical Review D* 71, 2005.
- [13] Sameie, O., Benson, A. J., Sales, L. V., Yu, H., Moustakas, L. A., and Creasey, P. The Effect of Dark Matter–Dark Radiation Interactions on Halo Abundance: A Press–Schechter Approach. *The Astrophysical Journal* 874, 2019, 101.
- [14] Schaeffer, T. and Schneider, A. Dark acoustic oscillations: imprints on the matter power spectrum and the halo mass function. *Monthly Notices of the Royal Astronomical Society* 5043, 2021, 3773–3786.
- [15] Marsh, D. Axion cosmology. *Physics Reports* 643, 2016. Axion cosmology, 1–79.
- [16] Schive, H.-Y., Chiueh, T., Broadhurst, T., and Huang, K.-W. Contrasting Galaxy Formation from Quantum Wave Dark Matter,  $\psi$ DM, with  $\Lambda$ CDM, Using Planck and Hubble Data. *The Astrophysical Journal* 8181, 2016, 89.
- [17] Hui, L., Ostriker, J. P., Tremaine, S., and Witten, E. Ultralight scalars as cosmological dark matter. *Physical Review D* 95, 2017, 043541.
- [18] Dentler, M., Marsh, D. J. E., Hlozek, R., Laguë, A., Rogers, K. K., and Grin, D. Fuzzy dark matter and the Dark Energy Survey Year 1 data. *Monthly Notices of the Royal Astronomical Society* 5154, 2022, 5646–5664.
- [19] Hsueh, J.-W., Enzi, W., Vegetti, S., Auger, M. W., Fassnacht, C. D., Despali, G., Koopmans, L. V. E., and McKean, J. P. SHARP– VII. New constraints on the dark matter free-streaming properties and substructure abundance from gravitationally lensed quasars. *Monthly Notices of the Royal Astronomical Society* 4922, 2019, 3047–3059.
- [20] Shirasaki, M., Ishiyama, T., and Ando, S. I. Virial Halo Mass Function in the Planck Cosmology. *The Astrophysical Journal* 922, 2021, 89.
- [21] Sippele, J., Lidz, A., Grin, D., and Sun, G. Fuzzy dark matter constraints from the Hubble Frontier Fields. *Monthly Notices of the Royal Astronomical Society* 5383, 2025, 1830–1842.
- [22] Despali, G., Vegetti, S., White, S. D. M., Powell, D. M., Stacey, H. R., Fassnacht, C. D., Rizzo, F., and Enzi, W. Detecting low-mass haloes with strong gravitational lensing I: the effect of data quality and lensing configuration. *Monthly Notices of the Royal Astronomical Society* 5102, 2022, 2480–2494.

[23] Wagner-Carena, S., Lee, J., Pennington, J., Aalbers, S., Birrer, S., and Wechsler, R. H. A Strong Gravitational Lens Is Worth a Thousand Dark Matter Halos: Inference on Small-scale Structure Using Sequential Methods. *Astrophysical Journal* 9752, 2024, 297–319.

[24] Keeley, R. E., Nierenberg, A. M., Gilman, D., Gannon, C., Birrer, S., Treu, T., Benson, A., Du, X., Abazajian, K., Anguita, T., Bennert, V., Djorgovski, S., Gupta, K., Hoenig, S., Kusenko, A., Lemon, C., Malkan, M., Motta, V., Moustakas, L., Maverick, S., Oh, H., Sluse, D., Stern, D., and Wechsler, R. JWST lensed quasar dark matter survey II. Strongest gravitational lensing limit on the dark matter free streaming length to date. *Monthly Notices of the Royal Astronomical Society* 5352, 2024, 1652–1671.

[25] Vegetti, S., Birrer, S., Despali, G., Fassnacht, C. D., Gilman, D., Hezaveh, Y., Perreault Levasseur, L., McKean, J. P., Powell, D. M., O’Riordan, C. M., and Verneratos, G. Strong Gravitational Lensing as a Probe of Dark Matter. *Space Science Reviews* 22058, 2024.

[26] Despali, G., Heinze, F. M., Fassnacht, C. D., Vegetti, S., Springola, C., Klessen, R., and Tajalli, M. Detecting low-mass haloes with strong gravitational lensing - II. Constraints on the density profiles of two detected subhaloes. *Astronomy & Astrophysics* 699, 2025, A222.

[27] Banik, N., Bovy, J., Bertone, G., Erkal, D., and de Boer, T. J. L. Novel constraints on the particle nature of dark matter from stellar streams. *Journal of Cosmology and Astroparticle Physics* 202110, 2021, 43–66.

[28] Barry, M., Wetzel, A., Chapman, S., Samuel, J., Sanderson, R., and Arora, A. The dark side of FIRE: predicting the population of dark matter subhaloes around Milky Way-mass galaxies. *Monthly Notices of the Royal Astronomical Society* 523, 2023, 428–440.

[29] Bonaca, A. and Price-Whelan, A. M. Stellar streams in the Gaia era. *New Astronomy Reviews* 100, 2025, 101713.

[30] Jones, M. G., Haynes, M. P., Giovanelli, R., and Moorman, C. The ALFALFA HI mass function: a dichotomy in the low-mass slope and a locally suppressed ‘knee’ mass. *Monthly Notices of the Royal Astronomical Society* 477, 2018, 2–17.

[31] Zhang, C.-P., Zhu, M., Jiang, P., Cheng, C., Wang, J., Wang, J., Xu, J.-L., Liu, X.-L., Yu, N.-P., Qian, L., Yu, H., Ai, M., Jing, Y., Xu, C., Liu, Z., Guan, X., Sun, C., Yang, Q., Huang, M., Hao, Q., and FAST Collaboration. The FAST all sky HI survey (FASHI): The first release of catalog. *Sci. China Phys. Mech. Astron.* 67, 2024.

[32] Garland, J. T., Masters, K., and Grin, D. Using HI observations of low-mass galaxies to test ultralight axion dark matter. *Monthly Notices of the Royal Astronomical Society* 535, 2024, 1338–1347.

[33] Bose, S., Hellwing, W. A., Frenk, C. S., Jenkins, A., Lovell, M. R., Helly, J. C., and Li, B. The Copernicus Complexio: statistical properties of warm dark matter haloes. *Monthly Notices of the Royal Astronomical Society* 4551, 2016, 318–333.

[34] Leo, M., Baugh, C. M., Li, B., and Pascoli, S. A new smooth-k space filter approach to calculate halo abundances. *Journal of Cosmology and Astroparticle Physics* 20184, 2018.

[35] Press, W. H. and Schechter, P. Formation of Galaxies and Clusters of Galaxies by Self-Similar Gravitational Condensation. *Astrophysical Journal* 187, 1974, 425–438.

[36] Bond, J. R., Cole, S., Efstathiou, G., and Kaiser, N. Excursion set mass functions for hierarchical gaussian fluctuations. *Astrophysical Journal* 379, 1991, 440–460.

[37] Sheth, R. K. and Tormen, G. An excursion set model of hierarchical clustering: ellipsoidal collapse and the moving barrier. *Monthly Notices of the Royal Astronomical Society* 3291, 2002, 61–75.

[38] Lukić, Z., Heitmann, K., Habib, S., Bashinsky, S., and Ricker, P. M. The Halo Mass Function: High-Redshift Evolution and Universality. *The Astrophysical Journal* 671, 2007, 1160–1181.

[39] Schneider, A., Smith, R. E., Maccio, A. V., and Moore, B. Non-linear evolution of cosmological structures in warm dark matter models. *Monthly Notices of the Royal Astronomical Society* 4241, 2012, 684–698.

[40] Benson, A. J., Farahi, A., Cole, S., Moustakas, L. A., Jenkins, A., Lovell, M., Kennedy, R., Helly, J., and Frenk, C. Dark matter halo merger histories beyond cold dark matter – I. Methods and application to warm dark matter. *Monthly Notices of the Royal Astronomical Society* 428, 2013, 1774–1789.

[41] Verwohlt, J., Mason, C. A., Muñoz, J. B., Cyr-Racine, F.-Y., Vogelsberger, M., and Zavala, J. Separating dark acoustic oscillations from astrophysics at cosmic dawn. *Physical Review D* 110, 2024, 103533.

[42] Schneider, A. and Trujillo-Gomez, S. Constraining cosmology with the velocity function of low-mass galaxies. *Monthly Notices of the Royal Astronomical Society* 475, 2018, 4809–4824.

[43] Kulkarni, M. and Ostriker, J. P. What is the halo mass function in a fuzzy dark matter cosmology? *Monthly Notices of the Royal Astronomical Society* 5101, 2021, 1425–1430.

[44] Schneider, A., Smith, R. E., and Reed, D. Halo mass function and the free streaming scale. *Monthly Notices of the Royal Astronomical Society* 4332, 2013, 1573–1587.

[45] Parimbelli, G., Scelfo, G., Giri, S., Schneider, A., Archidiacono, M., Camera, S., and Viel, M. Mixed dark matter: matter power spectrum and halo mass function. *Journal of Cosmology and Astroparticle Physics* 12, 2021.

[46] Cyr-Racine, F. Y., Sigurdson, K., Zavala, J., Bringmann, T., Vogelsberger, M., and Pfrommer, C. ETHOS—an effective theory of structure formation: From dark particle physics to the matter distribution of the Universe. *Physical Review D* 93, 2016, 123527.

[47] Coles, P. and Lucchin, F. *Cosmology: The Origin and Evolution of Cosmic Structure, 1st. Edition*. New York: John-Wiley & Sons, 1995.

[48] Zentner, A. R. The Excursion Set Theory of Halo Mass Functions, Halo Clustering, and Halo Growth. *Int. J. Mod. Phys. D* 165, 2007, 763–815.

[49] Mo, H., van den Bosch, F., and White, S. *Galaxy formation and evolution*. New York: Cambridge University Press, 2010.

[50] Maggiore, M. and Riotto, A. The halo mass function from the excursion set theory. I. Gaussian fluctuations with non-markovian dependence on the smoothing scale. *Astrophysical Journal* 711, 2010, 907–927.

[51] Sheth, R. K. and Tormen, G. Large-scale bias and the peak background split. *Monthly Notices of the Royal Astronomical Society* 308, 1999, 119–126.

[52] Bohr, S., Zavala, J., Cyr-Racine, F.-Y., and Vogelsberger, M. The halo mass function and inner structure of ETHOS haloes at high redshift. *Monthly Notices of the Royal Astronomical Society* 5061, 2021, 128–138.

[53] Brown, S. T., McCarthy, I. G., Stafford, S. G., and Font, A. S. Towards a universal model for the density profiles of dark matter haloes. *Monthly Notices of the Royal Astronomical Society* 5094, 2021, 5685–5701.

[54] Diemer, B. and Kravtsov, A. V. A Universal Model for Halo Concentrations. *The Astrophysical Journal* 7991, 2015, 108.

[55] Ludlow, A. D., Bose, S., Angulo, R. E., Wang, L., Hellwing, W. A., Navarro, J. F., Cole, S., and Frenk, C. S. The mass–concentration–redshift relation of cold and warm dark matter haloes. *Monthly Notices of the Royal Astronomical Society* 4602, 2016, 1214–1232.

[56] Lacey, C. and Cole, S. Merger rates in hierarchical models of galaxy formation. *Monthly Notices of the Royal Astronomical Society* 262, 1993, 627–649.

[57] Lewis, A., Challinor, A., and Lasenby, A. Efficient Computation of Cosmic Microwave Background Anisotropies in Closed Friedmann-Robertson-Walker Models. *The Astrophysical Journal* 538, 2000, 473–476.

[58] Murgia, R., Merle, A., Viel, M., Totzauer, M., and Schneider, A. “Non-cold” dark matter at small scales: a general approach. *Journal of Cosmology and Astroparticle Physics* 201711, 2017, 046.

[59] Bohr, S., Zavala, J., Cyr-Racine, F. Y., Vogelsberger, M., Bringmann, T., and Pfrommer, C. ETHOS – an effective parametrization and classification for structure formation: the non-linear regime at  $z \gtrsim 5$ . *Monthly Notices of the Royal Astronomical Society* 498, 2020, 3403–3419.

[60] Archidiacono, M., Bohr, S., Hannestad, S., Jorgensen, J. H., and Lesgourges, J. Linear scale bounds on dark matter-dark radiation interactions and connection with the small scale crisis of cold dark matter. *Journal of Cosmology and Astroparticle Physics* 2017, 2017, 010.

[61] Planck Collaboration et al. Planck 2018 results - VI. Cosmological parameters. *Astronomy & Astrophysics* 641, 2020, A6.

[62] Xu, Z. J. Dark matter halo mass functions and density profiles from mass and energy cascade. *Scientific Reports* 13, 2023, 16531.